Respiration Monitoring With RFID in Driving Environments

Chao Yang, *Student Member, IEEE*, Xuyu Wang, *Member, IEEE*, and Shiwen Mao, *Fellow, IEEE*

***Abstract*— To improve driving safety and avoid accidents caused by driving fatigue, drowsiness detection aims to alarm the driver before he/she falls asleep. Since breathing rate is a key indicator of the drowsy state, respiration monitoring in the noisy driving environment is critical for developing an effective driving fatigue detection system. In this paper, we propose, for the first time, an RFID based respiration monitoring system for driving environments. The system estimates the respiration rate of a driver based on phase values sampled from multiple RFID tags attached to the seat belt, while exploiting the *tag diversity* to combat the strong noise in the driving environment. Both tensor completion and tensor Canonical Polyadic Decomposition (CPD) are applied to process the phase values, to overcome the influence of frequency hopping, random sampling, vehicle vibration, and other environmental movements. The proposed system is analyzed and implemented with commodity RFID devices. Its accurate and robust performance is demonstrated with extensive experiments conducted in a real driving car.**

***Index Terms*— Radio-frequency identification (RFID), respiration monitoring, tensor decomposition, driving environment.**

I. Introduction

VEHICLES play a critical role in our society. With the drastic increase of the number of vehicles as well as driving time, driving safety has become ever more important than before. Driving fatigue is one of the primary causes of car accidents, which takes many lives every year [1]. It has been reported that there are on average 6 million car accidents in the U.S. every year [2], and more than 90 lives are lost every day. Such car accidents could be effectively avoided and human lives could be saved, if drivers are warned when they become sleepy. Drowsy driving can be indicated by multiple features of the driver, such as eyelid movements, driving movements, and human vital signs. Among various types of vital signs, respiration rate is a useful indicator of driver's fatigue state. It has been shown that the breathing rate usually decreases notably (i.e., for about 3 breaths per minute (bpm)) before the driver falls asleep [3]. Thus, accurately monitoring the respiration of the driver is a promising way, and the first step, to prevent drowsy driving. However, respiration monitoring for drivers is challenging, due to the highly strong noises in the driving environment, such as vehicle vibration and movements of the driver and passengers. Several techniques have been proposed for respiration monitoring using different types of signals, including video, ultra sound, and RF signals. Vision based methods detect respiration by analyzing the chest movements captured by a video camera [4], but it may not work well when lighting is poor (e.g., driving at night) and may raise privacy concerns. RF signals, such as WiFi [5] and UWB radar [6], have also been exploited, with the advantage of not requiring sufficient lighting inside the vehicle. However, due to the mutipath effect, such non-invasive RF sensors may be easily affected by the movements of driver and passengers. Recently, ultra sound signals generated by smartphones have been considered in [7]. Acoustic signals are shown to be effective to capture the human breathing signal [8], but as RF signals, they are also sensitive to the strong noises in the driving environment.

To this end, radio frequency identification (RFID) provides a promising alternative solution. RFID based sensing has become a hot problem area recently. Unlike other contact-free sensors, RFID tags are much cheaper and can be easily attached to the target object. As a near-field communication technology, it is more robust to surrounding noises. However, to exploit commodity RFID (rather than customized hardware) for respiration monitoring, many challenges should be addressed. For example, frequency hopping, as required by the Federal Communications Commission (FCC), causes large phase offsets, making received phase data useless. With the Slotted ALOHA medium access control protocol, the tags are sampled randomly, and it is common that the readings from the same tag are sparse (many are missing). There have been several recent works employing RFID for respiration monitoring [9]–[11], but *all the existing schemes work in a static indoor environment*. The strong interference from the driving environment prevents their application for driver respiration monitoring.

In this paper, we address the above challenges with novel, effective solutions, and propose an RFID based respiration monitoring system for the driving environment. Specifically, we propose to attach multiple tags to the driver's seat belt, which allow us to exploit the *tag diversity*. Although the same respiration signal is sampled by all the tags, the reader collected data is of high diversity as resulted from the multiple independent sampling. We also develop an effective tensor completion technique to mitigate the effect of frequency

Manuscript received December 6, 2019; revised January 11, 2020; accepted March 14, 2020. Date of publication August 31, 2020; date of current version January 15, 2021. This work was supported in part by the U.S. National Science Foundation (NSF) under Grants ECCS-1923717 and CNS-1822055, and in part by the Wireless Engineering Research and Education Center (WEREC) at Auburn University. *(Corresponding author: Shiwen Mao.)*

Chao Yang and Shiwen Mao are with the Department of Electrical and Computer Engineering, Auburn University, Auburn, AL 36849-5201 USA (e-mail: czy0017@tigermail.auburn.edu; smao@ieee.org).

Xuyu Wang is with the Department of Computer Science, California State University, Sacramento, CA 95819-6021 USA (e-mail: xuyu.wang@csus.edu).

Color versions of one or more of the figures in this article are available online at https://ieeexplore.ieee.org.

Digital Object Identifier 10.1109/JSAC.2020.3020606

hopping and random sampling. The recovered phase difference by tensor completion helps to combat the effect of vehicle vibration and driver/passenger body movements. Finally we apply tensor Canonical Polyadic Decomposition (CPD) to separate the small respiration signal from strong noises. The idea of increasing the dimension of data is essential to detect the weak respiration signal from noisy and sparse samples.

Specifically, we first provide an analysis of the sampled phase data that is used in the proposed system, and investigate the impact of frequency hopping offset as well as the challenges of respiration monitoring in driving environments. The proposed system is designed with several novel components to address these challenges, including data collection, data preprocessing, CPD, and respiration signal estimation. With multiple tags attached to the seat belt, the breathing signal can be effectively embedded in the phase data captured by the reader. However, the sampled phases are sparse due to random sampling, and are greatly distorted by channel hopping, vehicle vibration, and body movements. To combat such noises, we propose a High Accuracy Low Rank Tensor Completion (HaLRTC) based technique to estimate the phase difference between each pair of tags in each time slot, and to eliminate the frequency hopping effect simultaneously [12]. To extract a clean breathing signal, we leverage a CPD based technique to decompose the tensor data constructed by the previous estimated phase difference. Finally, the breathing signal is recovered from decomposed tensor data, and the breathing rate can be estimated with a peak detection algorithm.

The main contributions of this paper are summarized below.

- To the best of our knowledge, this is the first work on respiration monitoring in driving environments using commodity RFID reader and tags.
- We propose a tensor completion technique to recover missing readings in collected phase data, and a tensor decomposition approach to extract the respiration signal of the driver from phase values sampled from multiple RFID tags. The proposed techniques are effective in combating the strong noises caused by frequency hopping, random sampling, vehicle vibration, and other movements in the driving movement.
- We develop a prototype system with commodity RFID devices and test the system in real driving environments. Extensive experiments are conducted to evaluate the system performance in various driving scenarios, such as parked, in city streets, and on a highway, and system configurations, where a highly accurate and robust performance is demonstrated.

In the following, we review related work in Section II and present the preliminaries and system overview in Section III. The detailed system design is introduced and analyzed in Section IV. We present our experimental performance evaluation in Section V and conclude this paper in Section VI.

II. Related Work

This work is closely related to RF based vital sign monitoring and RFID based sensing. We mainly review these two classes of systems in this section.

RF based health sensing systems have been developed that employ Radar, WiFi, and RFID techniques. Radar based vital sign monitoring systems include frequency modulated continuous wave (FMCW) radar [13] and Doppler Radar [14]. However, they usually require customized hardware and operate over a wide spectrum. WiFi based systems mainly use received signal strength (RSS) and channel state information (CSI). For example, UbiBreathe [15] and mmVital [16] utilize WiFi RSS at 2.4 GHz and 60 GHz, respectively. To improve accuracy, CSI based systems leverage the amplitude or phase difference information of CSI for estimating single or multiple persons' breathing and heart rates [17]–[20]. Moreover, several bimodal CSI data based systems have been proposed to tackle the weak breathing signals at some special positions [21]–[23].

Recently, several RFID based breathing monitoring systems have been proposed. For example, RFID tags have been used for breathing rate estimation in [9], breathing and heart rates estimation in [24], and breathing monitoring and sleeping posture recognition in [25]. Furthermore, the RF-ECG system is proposed for heart rate variability assessment using an RFID tag array [26]. To mitigate the frequency hopping offset in FCC-compliant RFID systems, the AutoTag system is proposed for breathing monitoring and apnea detection with a variational autoencoder [10], [11]. However, these existing systems are designed for the indoor, static environment; they may not be effective in the highly dynamic, highly noisy driving environment.

Recently, WiFi based [5], acoustic based [7], and UWB based [6] systems have been developed for breath monitoring in driving environments. In fact, these existing systems are sensitive to the environmental interference, such as the body movements of the driver himself/herself and of the passengers, due to their relatively large transmission ranges.

In addition to vital sign monitoring, RFID tags have also been applied for many other applications, such as indoor localization [27], [28], user authentication [29], material identification [30], object orientation estimation [31], vibration sensing [32], anomaly detection [33], and drone localization and navigation [34], [35]. To overcome the low accuracy when RSS values are used [36], recent works are mainly focused on the phase for indoor localization, which can be used to derive the distance and direction of arrival (DOA). To solve the phase ambiguity problem, synthetic aperture radar (SAR) [37] and the hologram techniques [27], [38] are proposed. The RFind system estimates time-of-flight with a special hardware to achieve high localization precision [39].

This work, to the best of our knowledge, is the first to apply RFID based sensing for monitoring breathing signals in a driving environment. The proposed system consists of novel and effective solutions for noise and movement interference removal and breathing signal separation. The tensor based approach in this work has been analyzed and proven to be effective for the noisy driving environment.

III. Challenges and System Overview

A. Phase of the RFID Signal

To detect the breathing signal from received phase values from multiple RFID tags, we should firstly know how these

phase samples are collected by the RFID reader. In RFID systems, phase information is one type of low level data, which is collected when the RFID reader receives the Electronic Product Code (EPC) from interrogated tags. When the multipath effect is negligible, the measured phase sample can be written as [40]

$$\varphi = \mathrm{mod}\left(2\pi(2D)\cdot f/c + \varphi_{tag} + \varphi_T + \varphi_R, 2\pi\right), \quad (1)$$

where D is the distance between the sampled RFID tag and the reader antenna, f is the frequency of the currently occupied channel, and c represents the speed of light. Moreover, φ_{tag}, φ_T, and φ_R are the additional phase rotation for the tag, the transmitter, and the receiver, respectively. These additional phase rotations are mainly caused by the circuits in the reader and tag hardware. Furthermore, different reflection characteristics of these devices also contribute to the phase distortion.

This model implies that we could use phase values to detect the changes in the distance between the antenna and the tag. When the tag is attached to the human chest, the phase changes are indicative of the breathing signal. However, in addition to D, the other parameters, i.e., f, φ_{tag}, φ_T, and φ_R, are all susceptible to the current channel used by the reader. Thus, the measured phase value will have a different phase offset when the system hops to a new channel. Following FCC regulations, the Ultra-High Frequency (HUF) RFID system should hop among 50 channels within 10 seconds, so the sampled phase data will be heavily corrupted by frequency hopping. *The frequency hopping effect poses a big challenge for extracting the respiration signal.*

B. Respiration Monitoring in Driving Environments

To capture the respiration of a driver, we attach RFID tags on the seat belt, as illustrated in Fig. 1. Since the seat belt is bonded on the driver's body, it (and the tags) moves along with the rise and fall of the chest. Such movements are carried in the sampled phase values of each tag (see (1)), which will be captured by the RFID reader placed on the ceiling above the driver seat. *A big challenge is that, the seat belt/tag movements are no only caused by breathing, but also affected by other environmental factors in the car.*

Fig. 1 presents the sampled phase signal from a single RFID tag collected in different scenarios. For better illustration, the plotted phase data has already been preprocessed by removing the frequency hopping effect (to be discussed in Section IV-A). Theoretically, without the influence of channel hopping, the phase samples should exhibit the periodicity of human respiration. In fact, the collected phase signal, when the car is parked, exhibits strong periodicity. However, the sampled phase values in a moving vehicle, as shown in the second subplot in Fig. 1, are highly random, i.e., far from a periodic signal. This is because that respiration monitoring in a driving environment is very different from other respiration monitoring scenarios, in which the user is usually in a relative stable state, such as sleeping or sitting [10], [11], [19], [41]. This assumption does not hold true in driving environments. First, the vehicle vibrates when moving fast on the road, which makes the seat belt vibrate along with the car. Second, drivers

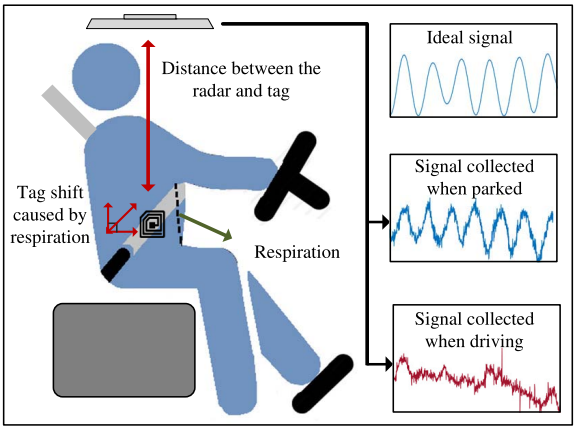

Fig. 1. Illustration of the respiration monitoring mechanism.

do not remain completely still. For example, the arms move when the driver turns the steering wheel, and the head moves when the drive looks around to check traffic conditions, which will cause additional movements to the tags. Such environmental movements also cause time-varying multipath interference by reflecting the RFID signal. Accordingly, *how to mitigate the impact of vehicle vibration and body movements poses another challenge (in addition to frequency hopping), to be addressed in our system.*

C. System Architecture Overview

To overcome the above challenges, we develop a tensor based breath monitoring system with an architecture shown in Fig. 2. The proposed system consists of four modules, including data collection, breathing data preprocessing, tensor decomposition, and respiration signal estimation.

In the *data collection module*, the reader keeps on interrogating the RFID tags attached to the seat belt and collecting phase samples from each tag. The *data preprocessing module* is to remove the channel hopping offset and to mitigate the noise from the driving environment. Since the raw phase data is corrupted by frequency hopping, it cannot be directly employed for breathing signal extraction. Fortunately, the phase variation within each individual channel is not affected by channel hopping; this fact is leveraged in our system to recover the phase data for a certain channel (see next section). Vehicle vibration mitigation is accomplished by calculating the recovered phase difference between a pair of tags. Since the vibration has a similar impact on the two tags, subtracting the phase data from the two tags can effectively mitigate the vehicle vibration noise. However, the challenge is that, the phase data is not sampled simultaneously from all the tags; there is only one phase reading from one of the tags in each time slot. To calculate the phase difference between two tags in each time slot, the missing phase sample(s) in the same time slot should be accurately estimated. To this end, we leverage a compressed sensing technique named HaLRTC to estimate the missing phase data [12], so that we can calculate accurate phase difference for each pair of tags.

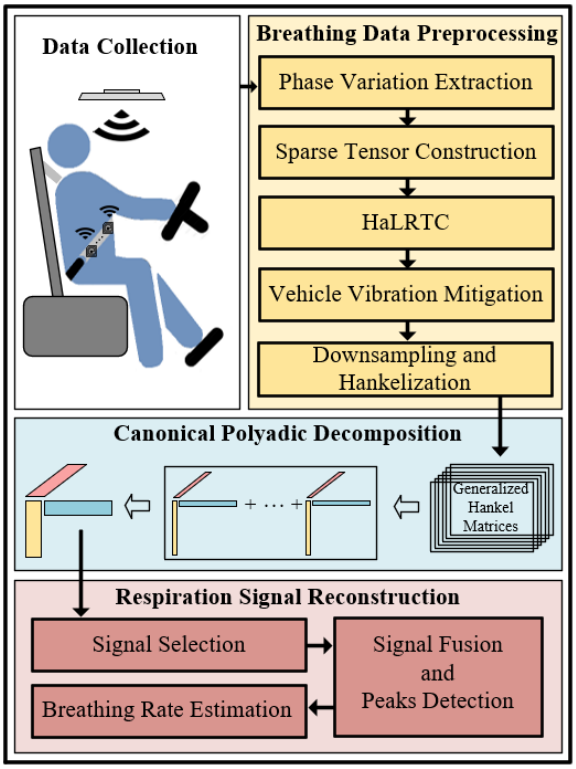

Fig. 2. Architecture of the proposed system.

Next, we hankelize all calculated phase difference values to construct a tensor for the following tensor decomposition module. After the phase difference tensor is constructed, we leverage CPD to extract the components related to driver's respiration. Finally, we recover the respiration signal of the driver by fusing all breathing related components and estimate the breathing rate with a peak detection algorithm. The system design will be elaborated and analyzed in the next section.

IV. System Design and Analysis

A. Combating Frequency Hopping Offset

The FCC regulation requires frequency hopping for UHF RFID systems. The phase offset generated by frequency hopping should be firstly removed in signal preprocessing. We rewrite (1) for the phases sampled from the 50 channels as

$$\varphi = \mathrm{mod}\left(4\pi D f_K/c + \varphi_K, 2\pi\right), \quad K = 1, 2, \ldots, 50, \quad (2)$$

where K is the channel index, f_K represents the frequency of channel K, and φ_K is the sum of φ_{tag}, φ_T and φ_R, because all these values are irrelevant to D but are affected by frequency hopping. From (2), we can see that the phase offset due to channel hopping is actually caused by f_K and φ_K.

Several techniques have been proposed to remove the effect of these two factors. For example, in AutoTag [10], the phase offset between two adjacent channels is estimated by the difference between the mean value near the end of the previous channel and that at the beginning of the next channel. This technique achieves a very good performance when the number of interrogated RFID tags is no more than 3. However, as the number of tags is increased, it would be hard to guarantee that enough samples can be collected from all the tags, which are needed for calculating the mean values. In addition, Tagyro leverages a full channel scan and calibration to measure φ_K in each channel [31]. The technique is suitable for RFID systems with more tags. In a driving environment, however, the estimated φ_K could be greatly affected by vehicle vibration and driver's body movement.

Since our system needs to interrogate at least 4 tags for tag diversity (see Section IV-B), we propose a novel approach to remove the channel hopping effect. If we subtract the sampled phase φ_n from the previous sampled phase φ_{n-1}, given in (2), we can obtain the nth *phase variation* on channel K as

$$v_n = 4\pi f_K (D_n - D_{n-1})/c, \quad (3)$$

where v_n represents the phase variation between the current and the previous phase sample, D_n is the antenna-tag distance in the nth sample. We find that the phase variations on the same channel are not related to the initial phase offset φ_K. With (3), we can easily translate the variations from all channels to a reference channel $\mathbb{R}$ by multiplying a factor $f_{\mathbb{R}}/f_K$. In fact, the reference channel can be any one of the 50 channels. In our system, we set $\mathbb{R} = 1$ to make channel 1 the reference channel for convenience. However, when the nth sample and the $(n-1)$th sample are not from the same channel, Eq. (3) should be updated as

$$v_n = 4\pi (f_K D_n - f_{K-1} D_{n-1})/c + \varphi_K - \varphi_{K-1}. \quad (4)$$

Eq. (4) shows that when two adjacent phase samples are not collected from the same channel, the phase variation is still affected by the initial phase offsets of the two different channels. To mitigate the frequency hopping offset, we should drop these distorted phase variations. Fortunately, since only a single phase variation is affected once the system hops to a new channel, most of the remaining data are still usable. Such results are illustrated in Fig. 3. We calculate the phase variation from the raw, sampled phase data, and delete the distorted phase variations when hopping to a new channel. It can be observed that although the phase is corrupted by frequency hopping (the upper plot), the phase variation is confined within $[-0.15$ rad, 0.1 rad$]$. This result shows that most of the phase variations are not affected by channel hopping.

B. Recovering Phase for Each Time Slot

To combat vehicle vibration, we propose to leverage the phase difference between two tags. However, following the Gen2 protocol [40], when one tag is sending its EPC to the reader, all other tags should remain silent to avoid collision. The random sampling details are illustrated in Fig. 4, which shows the phase data sampled by the reader from multiple tags. A colored square indicates that a valid phase value is sampled from the tag, a blank square means the tag is not sampled in that time slot, and all the same colored squares are sampled from the same channel. Because the entire transmitting process is based on slotted ALOHA, the tags are sampled randomly. That is, phase can be collected from only one tag in each time slot, and the sampling interval for each tag is random.

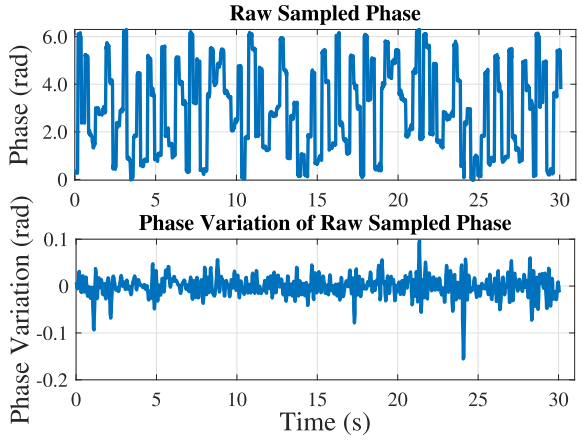

Fig. 3. Raw phase and the filtered phase variation signal.

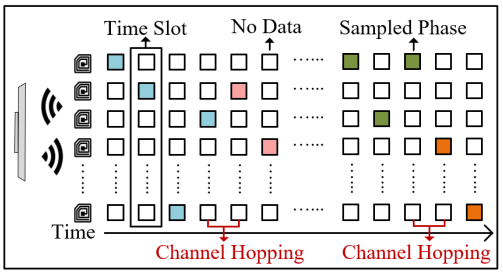

Fig. 4. Slotted ALOHA based random sampling in RFID systems.

Because calculating phase difference between two tags requires to sample phase data from both tags in the same time slot, we need to estimate the missing phase data of all tags in every time slot, i.e., the blank squares in Fig. 4. Several compressed sensing approaches have been shown to achieve a good performance on recovering the missing RFID phase data [42], [43], where the number of deployed tags are less than 3. For example, in [42], a missing phase is estimated from neighboring sampled phase values with a Blackman window, where a pair of tags are used. However, these existing techniques are not suitable for our system, where more tags are deployed. When there are more tags, the sparsity of data becomes higher, thus resulting in a lower recovering accuracy.

Tensor completion is another powerful tool of compressed sensing, which has been adopted to recover missing data in RFID systems in our recent work [44]. We propose a tensor completion based method to recover the phase sequences for all tags in every time slot. Rather than directly recovering the phase sequence as in [44], we recover the sequence of *phase variation* for each tag, and then calculate phase by integrating the recovered phase variation. This is motivated by the fact that phase variation is not affected by frequency hopping, as proven in Section IV-A.

We first define the *ideal matrix* we aim to recover, given by

$$V_T \doteq \begin{bmatrix} v_{1t_1} & v_{1t_2} & v_{1t_3} & \dots & v_{1t_n} \\ v_{2t_1} & v_{2t_2} & v_{2t_3} & \dots & v_{2t_n} \\ \vdots & \vdots & \vdots & \vdots & \vdots \\ v_{mt_1} & v_{mt_2} & v_{mt_3} & \dots & v_{mt_n} \end{bmatrix}, \tag{5}$$

where m is the tag index, t_n is the nth time slot, and v_{mt_n} is the real phase variation of tag m at time t_n. Due to slotted ALOHA, only one value in each column of V_T can be sampled. The goal is to estimate a matrix $\hat{V}_T$, such that $\hat{V}_T \approx V_T$, based on collected sparse samples. We first build a *sampled matrix* $\bar{V}_T$, which is of the same size as V_T, but all the missing data elements are set to 0. We then filter out thermal noise from the phase variation signal using a low-pass filter with a 15 Hz cutoff frequency, and map the signal to the sampled elements in $\bar{V}_T$. Moreover, all the distorted phase variations in $\bar{V}_T$ that satisfy (4), are also set to 0 (i.e., dropped) to avoid the influence of frequency hopping.

In the proposed system, 4 to 8 tags are attached to the seat belt and the frequency of time slots is about 220 Hz, which means the sparsity of $\bar{V}_T$ is higher than 75%, and the number of columns is much larger than the number of rows. Because of the high sparsity and the limited number of rows, the traditional singular value decomposition (SVD) based matrix completion method would not be effective for such $\bar{V}_T$, Therefore, we transform the data into a tensor form and apply tensor completion to estimate the missing data. Specifically, we reshape each row into a *generalized* Hankel matrix as the frontal slice of the tensor, which has the same format of Hankel matrix but is not square. The sparse matrix $\bar{V}_T$ is thus transformed into a tensor, given by

$$\bar{\mathcal{V}}_{(:,:,m)} \doteq \begin{bmatrix} v_{mt_1} & v_{mt_2} & \dots & v_{mt_{(n-r+1)}} \\ v_{mt_2} & v_{mt_3} & \dots & v_{mt_{(n-r+2)}} \\ \vdots & \vdots & \vdots & \vdots \\ v_{mt_r} & v_{mt_{(r+1)}} & \dots & v_{mt_n} \end{bmatrix}, \tag{6}$$

where r denotes the number of rows of the generalized Hankel matrix. Note that a large row number in Hankelization will lead to high complexity, while a small number of rows (i.e., less than 10) could considerably affect the recovering accuracy. Thus, we set $r = 20$ in our system (see Section V-B.6).

Since thermal noise is filtered before tensor construction, the ideal tensor $\mathcal{V}$, which is constructed by the ideal phase variation matrix V_T, can be considered as low rank data. Thus, $\mathcal{V}$ can be estimated from the sampled sparse tensor $\bar{\mathcal{V}}$ by low-rank tensor completion, which is accomplished by solving the following optimization problem [45]:

$$\min_{\hat{\mathcal{V}}} \|\hat{\mathcal{V}}\|_*, \quad \text{s.t.} \quad \Omega * \hat{\mathcal{V}} = \Omega * \bar{\mathcal{V}}, \tag{7}$$

where $\hat{\mathcal{V}}$ is an estimate of the ideal tensor $\mathcal{V}$, and Ω is a tensor of 0 and 1 elements, where $\Omega_{ijk} = 1$ when $\bar{\mathcal{V}}_{ijk}$ is sampled, and $\Omega_{ijk} = 0$ otherwise. $\|.\|_*$ denotes the trace norm of tensor [45]. We adopt the HaLRTC algorithm for tensor completion, which can solve the optimization problem (7) with the Augmented Lagrange Multiplier Method (ADMM) [12]. Compared with other tensor completion algorithms, HaLRTC usually achieves a higher accuracy at an acceptable complexity. A comparison of HaLRTC and a classic matrix completion method on phase variation recovery is shown in Fig. 5.

To make the comparison, we interrogate a single tag for 10 s, and repeat for 5 times as if there were 5 virtual tags. Since there is only one tag being interrogated each time, no data will be missing in V_T. We thus obtain the ideal phase

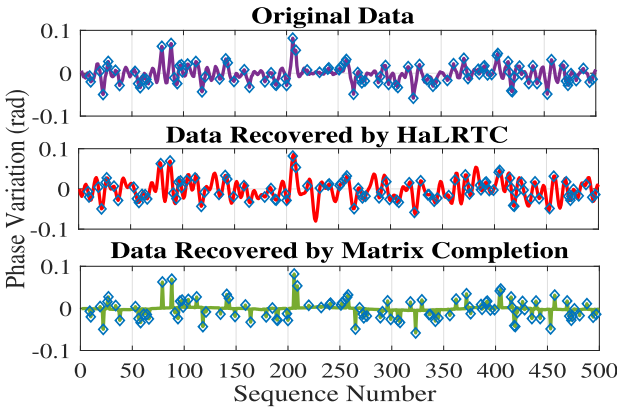

Fig. 5. Recovered signals using HaLRTC and Matrix Completion.

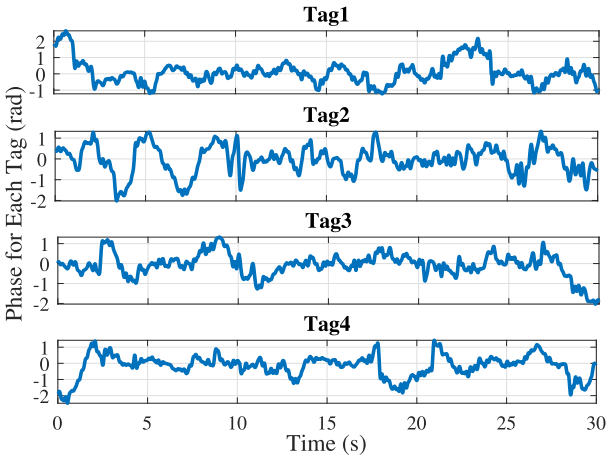

Fig. 6. Recovered phase after DC removal.

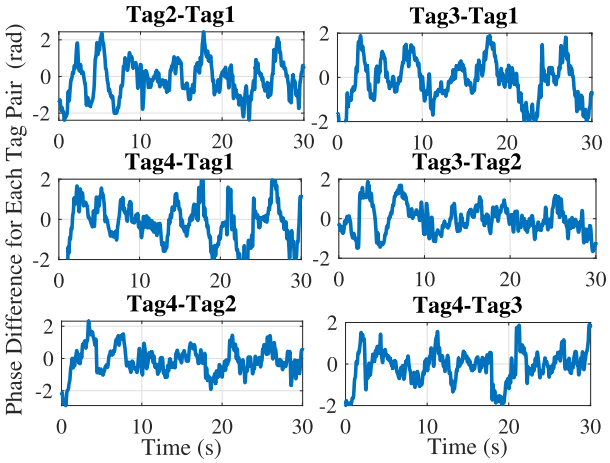

Fig. 7. Phase difference for each pair of RFID tags.

variation data V_T as ground truth, and then remove some elements in V_T according to the slotted ALOHA protocol to obtain $\bar{V}_T$. The remaining elements used for recovery are marked with $\diamond$ in Fig. 5. Since there are 5 virtual tags in the emulated data, the sparsity is higher than 80%. Fig. 5 shows the first 500 samples recovered by tensor completion and matrix completion, respectively. It can be seen that the recovered signal by HaLRTC is very similar to the original signal, while the recovered signal by matrix completion is not good. Many values recovered by matrix completion are still very close to 0. This is because there are only 5 rows in $\bar{V}_T$, but the number of columns is now 500. SVD based matrix completion cannot obtain sufficient singular values for accurate estimation. In contrast, although tensor completion also requires singular values for estimation, the unfolding process can provide a sufficient matrix size for decomposing singulars values.

Once $\hat{V}_T$ is successfully recovered by HaLRTC, we can easily recover the phase sequence of each tag for all time slots by integrating the corresponding phase variations. Furthermore, the recovered phase data will not be affected by frequency hopping, because all the distortion related phase variations are deleted when building $\bar{V}_T$.

C. Dealing With Vehicle Vibration and Body Movements

Interference caused by vehicle vibration and body or environment movements is another big challenge for breath monitoring in driving environments, which should be mitigated before tensor decomposition. The driving movement could have different impacts for different tags, because the tags are deployed at different parts of the seat belt. Fortunately, most of the driving related body movements are not fast, and the resulting interference can be considered as a direct current (DC) component (with frequencies around 0) in the recovered phase signal. We thus apply a Hampel filter with a windows size of 3 s and a threshold of 0.001 to extract the DC component and then subtract it from the original signal.

The filtered signals from 4 tags are illustrated in Fig. 6. We find that the DC components are successfully removed, but the respiration signal is still hard to see. This is because the phase signals are also influenced by vibration of the moving vehicle. The noise generated by vibration is hard to be estimated, because both strength and frequency of the noise are related to road conditions and speed of the car.

However, since all the tags are attached to the seat belt, the noise generated by vibration has a similar effect on them. With filtered recovered phase variation signal, we can obtain the *phase difference* for each tag pair in each time slot. The resulting phase difference is plotted in Fig. 7, where most phase difference curves exhibit strong periodicity, meaning the influence of vibration has been effectively mitigated.

D. CPD Based Respiration Signal Separation

1) Tensor Data Construction With Hankelization : Extracting a clean respiration signal from the calibrated phase difference data for different tag pairs, as shown in Fig. 7, is still challenging, because the periodicity strength of different tag pairs could vary with the movements of the driver and in the driving environment. It means no such tag pairs that could always reveal the highest periodicity, and the worst pairs could have no periodicity in the estimated phase difference. Some traditional signal processing techniques, such as discrete wavelet transform (DWT), can extract the respiration signal

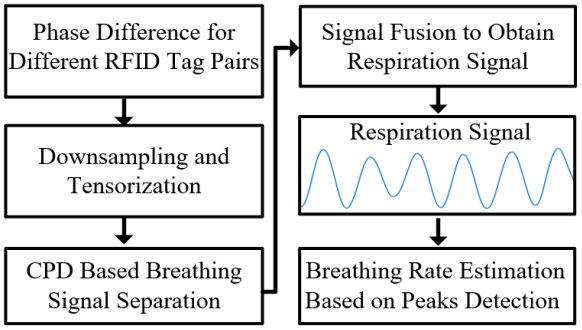

Fig. 8. Flow-chart of the CPD based respiration extraction method.

from the signal with sufficient periodicity, but the performance could be poor when DWT is applied to noisy signals.

However, since the respiration signal captured by phase difference is the same for all tag pairs, each phase difference sequence can be considered as the same respiration signal corrupted by different noises. Rather than employing signal processing techniques for each individual tag pairs, we can analyze the entire group of estimated phase difference data. Tensor decomposition is widely used to separate a correlated signal from multiple datasets [19], [46]. For example, in TensorBeat [19], CPD is used to separate multiple breathing signals from WiFi phase difference data. We can decompose the breathing signal from noises in driving environments using a *CPD tensor decomposition* method. The detailed process of respiration signal extraction is shown in Fig. 8.

As Fig. 8 shows, the respiration signal is extracted from the separated signals from CPD, so that the breathing rate could be estimated based on the interval of the detected signal peaks. Before decomposing the data with CPD, we transform the phase difference matrix into a tensor structure, by reshaping each phase difference sequence into a generalized Hankel matrix. Hankelization is essential before CPD decomposition is applied, because its special structure helps to separate a periodic signal (i.e., the breathing signal) from the data. We summarize the relationship between periodic signals and the proposed Hankel matrix in Theorem 1. The proof is provided in Appendix A.

Theorem 1: If the generalized Hankel matrix $\boldsymbol{H}$ with r rows is constructed from a sinusoidal wave with length n, it can be decomposed as: $\boldsymbol{H} = \sum_{i=1}^{2} \alpha_i \cdot \beta_i^T$, where both $\alpha_i \in \mathbb{R}^{r,1}$ and $\beta_i \in \mathbb{R}^{(n-r+1),1}$ represent sinusoidal signals with the same frequency as the original signal.

Theorem 1 provides the theoretical underpinning for estimating respiration rate from the generalized Hankel matrix derived from the phase difference sequence. It also determines the number of sinusoidal components to be decomposed from the generalized Hankel matrix. In our system, we build the generalized Hankel matrix with 30 s of data and leverage 10 s of data to build each column of the matrix. This is because 10 s of data can guarantee that at least one full period of the breathing signal can be decomposed in α_i.

2) CPD Based Breathing Signal Separation : With the tensor constructed by Hankelization, denoted by Γ, the respiration signal can be separated from noise by applying CPD, which decomposes the tensor into a sum of the outer products of three vectors as [47]

$$\Gamma \in \mathbb{R}^{I,J,K} \approx \sum_{m=1}^{M} \vec{a}_m \circ \vec{b}_m \circ \vec{c}_m, \tag{8}$$

where M is the tensor rank used for CPD, which also indicates the number of components in the decomposition result; $\vec{a}_m$, $\vec{b}_m$, $\vec{c}_m$ are the vectors at the mth position for the three dimensions, respectively. We have $\vec{a}_m \in \mathbb{R}^{I,1}$,$\vec{b}_m \in \mathbb{R}^{J,1}$, $\vec{c}_m \in \mathbb{R}^{K,1}$, and $(\vec{a}_m \circ \vec{b}_m \circ \vec{c}_m)(i,j,k) = \vec{a}_m(i)\vec{b}_m(j)\vec{c}_m(k)$, for all i, j, k. According to the definition of outer product, we can construct the matrix from the vectors for each dimension. For example, matrix $\boldsymbol{A}$ is defined as $[\vec{a}_1, \vec{a}_2, \ldots, \vec{a}_M]$, and matrices $\boldsymbol{B}$ and $\boldsymbol{C}$ are defined similarly with $\vec{b}_m$ and $\vec{c}_m$, respectively. The process of CPD is implemented by solving the following optimization problem.

$$\min_{\boldsymbol{A},\boldsymbol{B},\boldsymbol{C}} \|\Gamma - \sum_{m=1}^{M} \vec{a}_m \circ \vec{b}_m \circ \vec{c}_m\|_F^2. \tag{9}$$

Although the above problem is not convex, CPD leverages the Alternating Least Squares (ALS) algorithm to optimize one matrix while fixing the other two. With the ALS algorithm, the optimization problem can be reduced to a linear least squares problem, and the three matrices can be finally estimated.

In CPD, the number of components M should be prescribed, which is determined by the target signal and the uniqueness of the decomposition. Thus, we propose Theorem 2 to determine the range of M, which is proved in Appendix A.

Theorem 2: The tensor rank used for CPD in the proposed system should satisfy $2 \leqslant M \leqslant 4$ and the CPD is unique.

The noise in the tensor is usually considerably large in driving environments (i.e., much larger than the respiration signal). Some other noise components could also be decomposed. To separate noise and precisely extract the respiration signal, we set $M = 4$ for CPD. The decomposed matrix $\boldsymbol{B}$ is illustrated in Fig. 9. We can see that two sinusoidal signals with the same period are decomposed by CPD (i.e., the 3rd and 4th components), while the other components (i.e., the first and 2nd components) are for the residual noise after data preprocessing.

E. Breathing Rate Estimation

With the respiration signal separated by CPD, we can estimate the breathing rate using a peaks detection algorithm. However, we still need to differentiate the periodic signal from all decomposed signals before we estimate the breathing rate. Thus, we leverage a frequency spectrum based method to figure out which decomposed signal is for the breathing signal. We first calculate the proportion of the power spectrum between 0.2 Hz and 0.5 Hz in the frequency domain, which is the range of normal human breathing. Then, we search for the two signals with the first two largest proportions and fuse them to obtain the final breathing signal. The fused signal is illustrated in Fig. 10. It can be seen that the respiration signal is precisely extracted and the noises from vehicle vibration and other movements in the driving movement are effectively

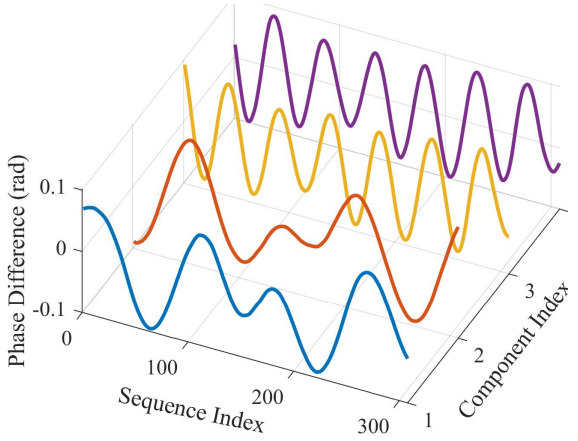

Fig. 9. Decomposed signals by CPD.

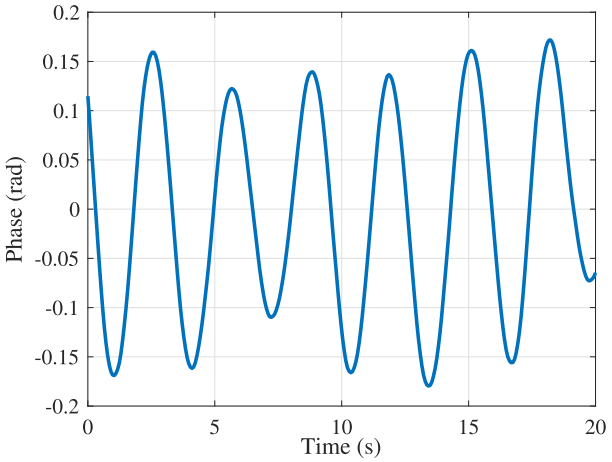

Fig. 10. Signal fused by all breathing related components.

removed. The intervals τ between each pair of adjacent peaks are calculated and the breathing rate F is determined by the average interval τ_{ave} as $F = 60/\tau_{ave}$.

V. System Performance Evaluation

A. Experiment Configuration

To evaluate the performance of our respiration monitoring system in the driving environment, we implement a prototype system with an Impinj R420 reader equipped with a polarized antenna S9028PCR.[1] The setup up of the system is illustrated in Fig. 11. As the figure shows, multiple ALE-9470 RFID tags are attached to the seat belt of the driver. The size of the polarized antenna utilized in the system could be smaller, because many small-sized antennas have been developed, such as Keonn Advantenna-p11 and Thingmagic EL6E.

Although the cost of the RFID reader used in the prototype system is not very low, some other cheaper readers could be adopted for reduced cost. For example, since only one antenna is required in our system, one port reader like

[1]Although we used such commodity RFID devides in our proof-of-concept prototyping and experiments, the size of the system can be greatly reduced by using smartphones with an attached reader, e.g., made by Zebra.

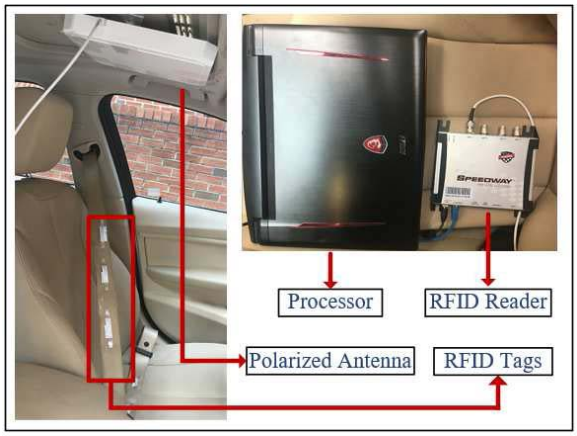

Fig. 11. Illustration of the system setup in a car in our experiments.

Impinj R120 can be used. Furthermore, medium range readers, such as Feig MRU102-PoE, will be another low-cost option, because the interrogate range for car environment monitoring is not demanding. Furthermore, our system is currently composed of multiple commodity devices. The cost of the future system could be further reduced, if customized readers are used and mass produced.

The channel used by the reader hops every 0.2 s among 50 channels from 902 MHz to 928 MHz when interrogating RFID tags. The processor used for signal processing is an MSI laptop with a Navidia GTX 1080 GPU and Intel Core i7-6820HK CPU. The model of the test vehicle is BMW 328i. Five volunteers (1 female and 4 males) are tested with our prototype system. The breathing rates of the volunteers are also estimated by a NEULOG sensor, which is considered to be the ground truth in our experimental result analysis.

B. Results and Discussions

1) Overall Accuracy for Different Rates: Our system is tested by five volunteers with different breathing rates. The cumulative distribution function (CDF) of estimation errors is presented in Fig. 12. The figure shows that the median errors for the three ranges of breathing rates are 0.11 bpm, 0.12 bpm, and 0.14 bpm, respectively, which are all very close to each other. However, the maximum error for the $10 \sim 15$ bpm range is 0.33 bpm, which is much smaller than that for the $16 \sim 23$ bpm range and that for the $24 \sim 30$ bpm range. This implies that the accuracy of the system is higher when the driver breaths slowly. This is because breathing rate is calculated by $F = 60/\tau_{ave}$, where τ_{ave} is estimated by peak detection. As the driver's breathing gets faster, τ_{ave} will become smaller, and the estimation error in τ_{ave} will be amplified in F.

We next compare with the traditional RFID based method presented in [10], [11] in Fig. 13, when the driver is driving on a highway (i.e., interstate I-85). Other RFID based respiration monitoring techniques, such as Tagbreathe [9], can achieve high accuracy in a stationary testing environment. However, the Tagbreathe system is not well suited for operation with Ultra High Frequency (UHF) RFID devices in the US,

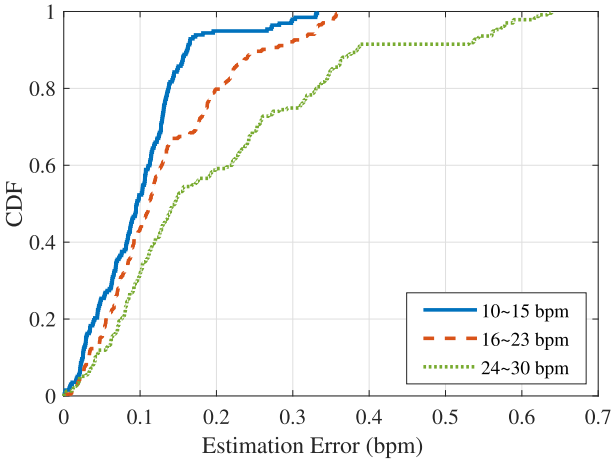

Fig. 12. System performance for different breathing rates.

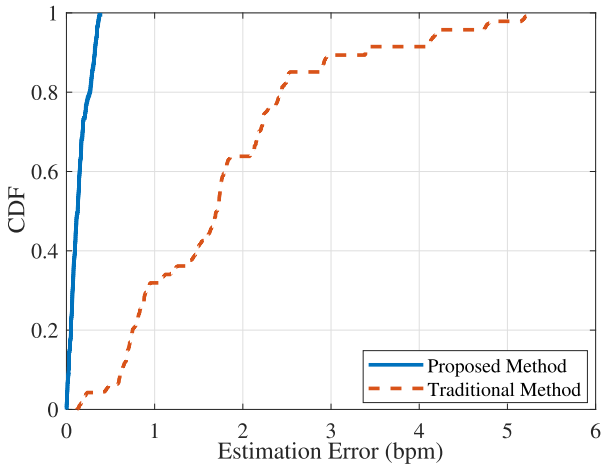

Fig. 13. System performance compared with a traditional RFID based respiration sensing technique for stationary environments [10], [11].

which requires frequency hopping. Thus, we only provide the experimental result of the RFID breathing monitoring system in a stationary environment proposed in [10], [11] to illustrate the robustness of our system in noisy driving environments.

The CDFs of estimation errors achieved by the traditional and proposed methods are presented in Fig. 13. We find that the median error of the traditional method is 1.71 bpm and 36.11% data has an estimation error larger than 2 bpm. In contrast, the median error of our proposed method is 0.12 and the maximum error is 0.36 bpm. From the results, we can conclude that the performance of the traditional method is quite limited in driving environments, because of the considerable interference caused by the vehicle, driver, and passengers. However, due to effective noise mitigation, our proposed method can achieve high accuracy in respiration monitoring in such noisy environments.

To compare the accuracy of breathing rate estimation for different types of systems, we summarize the mean estimation error as provided in related papers [4], [6] in Table I (note that we compare mean error rather than median error here, since those are provided in the two related papers). As shown in the

TABLE I

COMPARISON OF DIFFERENT BREATHING RATE MONITORING SYSTEMS FOR THE DRIVING ENVIRONMENT

Employed Device	*Mean Estimation Error*
Video Camera (Kinect)	0.79 bpm
UWB Radar	0.31 bpm
RFID Tags and Reader	0.11 bpm

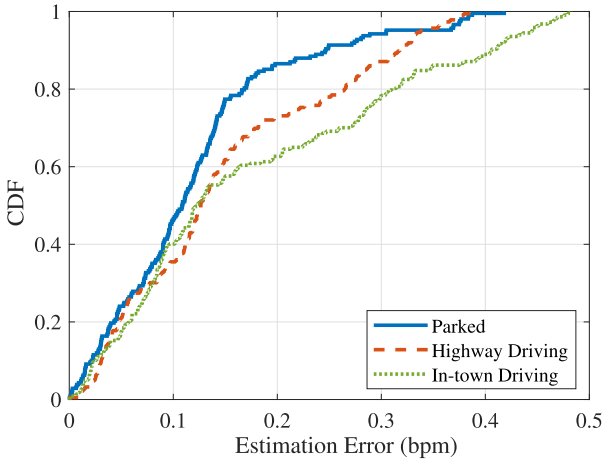

Fig. 14. System performance for different driving scenarios.

table, the video camera based method and UWB radar based method have higher estimation errors, which are 0.79 bpm and 0.31 bpm, respectively. The mean estimation error of the proposed system is 0.11 bpm, which is much lower than the other two. This is because RFID tags can provide high accuracy as wearable sensors, and the effect of interference from other passengers is limited too. Moreover, with measured phase from multiple RFID tags, the CPD based approach can effectively mitigate the influence of vehicle vibration and other noises in driving movements.

2) Accuracy in Different Driving Scenarios: The system is evaluated in 3 different scenarios, including (i) driving on a highway, (ii) driving in a city street, and (iii) parked. The CDF of errors for the three scenarios are plotted in Fig. 14. The median error is 0.11 bpm for the parked scenario and 0.12 bpm for the two driving scenarios. It proves that the influence of the driving environment is effectively mitigated by the proposed scheme. The figure also shows that the maximum error for in-town driving is 0.48 bpm, which is the highest among the three scenarios. This is because the driver needs to turn the wheel frequently and stops from time to time when driving in town, and the influence of the driving movements cannot be completely eliminated.

3) Impact of Passenger Movement: We also test the performance of our system when there are different numbers of passengers. In these experiments, all the passengers are asked to move naturally. As Fig. 15 shows, when no passenger is present, the median error is 0.09 bpm, which is the smallest among all the cases. The error increases to 0.11 bpm when there is one passenger in the car. The movement of the passenger does affect the sampled phase data, although the

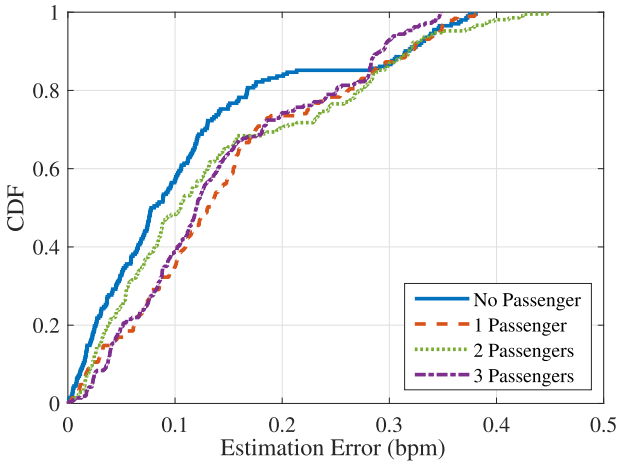

Fig. 15. System performance with different numbers of passengers.

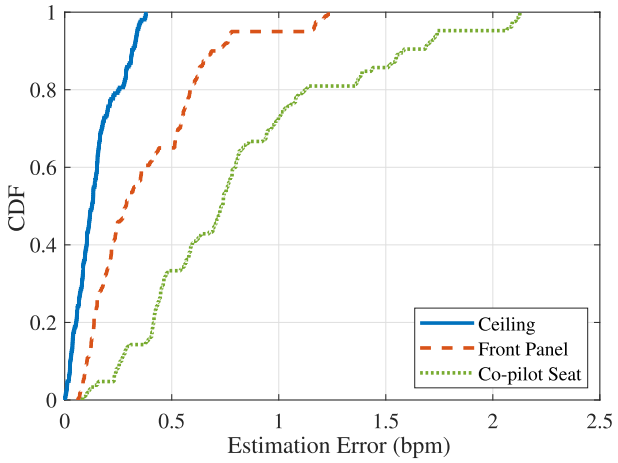

Fig. 16. System performance under different deployment locations of the polarized antenna.

impact is small. The median error is not obviously affected by increased number of passengers, and the maximum errors are almost the same for the different cases. This result shows that the performance of our system is not sensitive to the movement of passengers, because the tags are only attached to the seat belt of the driver as well as the near-field nature of RFID communications.

4) Impact of Antenna Position: We try different antenna deployment in our experiments to identify the most suitable way to place the antenna. The first scenario is to attach the antenna on the ceiling above the driver seat, as shown in Fig. 11. The second deployment is to attach the antenna to the front control panel of the vehicle. The third scenario is to bond the antenna on the side of the back of the co-pilot seat. The CDF results are plotted in Fig. 16. It can be seen that the deployment of the antenna has a considerable impact on the system performance. The median error is 0.73 bpm when the antenna is placed on the side of the diver, because the phase changes caused by the movement of human chest is harder to detect. The accuracy is also not high when the antenna is attached to the front panel, with a median error of 0.28 bpm. This is because the range of the polarized antenna is limited, and some of the tags cannot be scanned by the antenna. Thus, we conclude that the best deployment position of the antenna is the ceiling, which can guarantee full-tag interrogation and high sensitivity of detecting the respiration signal.

5) Impact of Number of Tags and Coupling Effect: We next evaluate the accuracy of our system with different numbers of tags. Since we need to calculate phase difference between tag pairs and build the tensor data, the minimum number of tags is 3 in our system. Fig. 17 shows the accuracy under different numbers of tags. The mean error is relatively high when only 3 tags are deployed, which is 0.45 bpm. This is because the 3 tags can only generate 3 phase difference sequences for CPD. The respiration signal is hard to be decomposed from the small tensor constructed by 3 tags. We also observe that when 5 or more tag are deployed, the error is reduced to 0.11 bpm. However, the error becomes 0.21 when 9 tags are used, because the error in recovering the missing samples

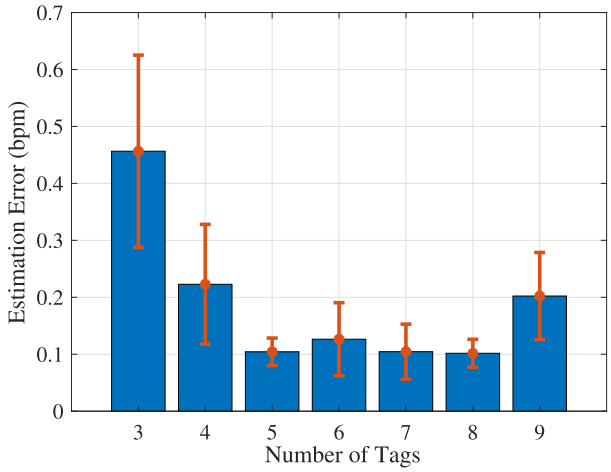

Fig. 17. Estimation error for different numbers of deployed tags.

becomes large with 9 tags. Moreover, more time will be consumed in data recovering and tensor decomposition when more tags are used. We use 5 tags on the seat belt in our system.

Fig. 17 also shows that the accuracy of the system is not seriously affected by the coupling effect, because the estimation error remains small (around 0.11 bpm) even when 8 tags are used. With 8 tags attached to the seat belt, the density of RFID tags is quite high, which generates large mutual coupling among these tags. Fortunately, the coupling effect only affects the phase value received by the reader [31], while the breathing rate estimation is dependent on the periodicity of the signal. Thus the system is robust to the mutual coupling effect. The figure also shows that, the error increases a little (to 0.2 bpm) when 9 tags are deployed. This is because the considerable larger mutual coupling effect may introduce low backscattering power from the tags in this case. Since the reader uses a power threshold for receiving tag response, tags with low backscattering power will hardly be interrogated by the reader. To make sure that all tags can provide enough

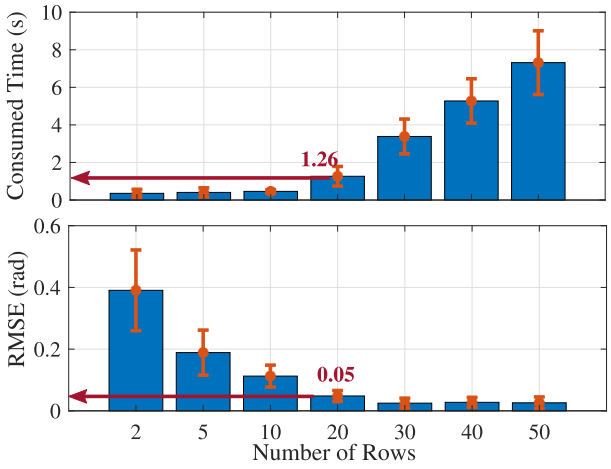

Fig. 18. Impact of Hankelization size on HaLRTC complexity and recovering accuracy.

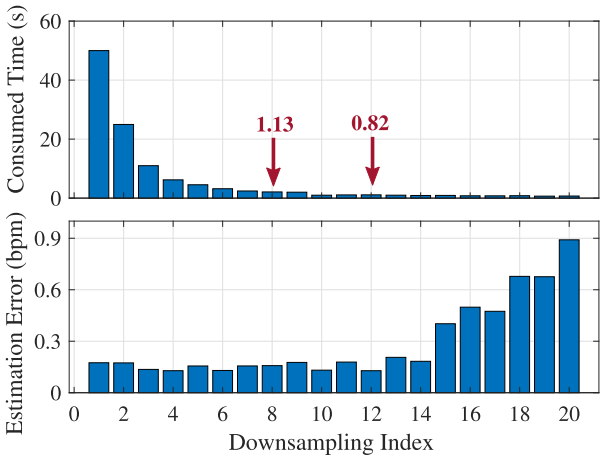

Fig. 19. Impact of downsampling on CPD complexity and system performance.

information to the reader, we conclude that 8 tags are the maximum number of tags for the prototype system.

6) Complexity Reduction: Since the system requires solving two optimization problems for data recovery and tensor decomposition, the complexity of the algorithm could be a problem that needs to be investigated. We aim to reduce the complexity of HaLRTC and CPD by reducing the size of the tensors and by downsampling. For phase recovery, we can reduce the size of the tensors by adjusting the number of rows in Hankelization. We utilize the 20 s data used in Fig. 5 to test the influence of the number of rows on complexity and accuracy. The results are shown in Fig. 18. We can see that as the number of rows is increased, the consumed time increases exponentially, while the Root Mean Square Error (RMSE) decreases exponentially. To trade off between accuracy and complexity, we choose 20 as the row number for building generalized Hankel matrix.

Downsampling is not implemented in the phase recovering process, because the sparsity of the data is very high and downsampling could considerably affect the recovery performance. However, downsampling is an effective way to reduce the complexity of CPD. Following Theorem 1, the rows of the generalized Hankel matrix in CPD should be large enough, or the periodicity of the signal can hardly be revealed in α_i. Thus, we fix the number of rows and test the performance of CPD with different downsampling indices. As Fig. 19 shows, when the index is larger than 12 the consumed time by CPD is shorter than 0.82 s, and the estimation error is smaller than 0.2 bpm when the index is smaller than 14. When the downsampling index gets higher, the accuracy decreases sharply, because the remaining data is not enough for CPD to precisely separate the breathing signal. To achieve high accuracy with an acceptable complexity, we downsample the data by 12 before constructing the tensor input for CPD.

In conclusion the total time consumed for data processing in our system is about 2 s. Since drowsy driving is a relatively long, slowly developing process (i.e., people do not fall asleep suddenly), such a latency should be sufficient to warn the driver in advance (e.g., the safe distance to the vehicle ahead of one's car is 2 or 3 s). In addition, the processing speed can be improved by specific embedded hardware. The complexity of the prototype system is acceptable.

VI. Conclusion

In this paper, we proposed an RFID based respiration rate monitoring system for the driving environment. The proposed system included several novel components, including data collection, breathing data preprocessing, CP tensor decomposition, and respiration signal estimation, to combat the strong noise caused by frequency hopping, random sampling, vehicle vibration, and other movements in the environment. The proposed system was implemented with commodity RFID tags and reader, and was evaluated under real driving scenarios. Our experiments showed that the tensor completion and CPD approaches were effective for respiration monitoring in driving environments.

Appendix A
Proof and Discussion of the Theorems in CPD Processing

A. Proof of Theorem 1

Proof: To analyze the features of the generalized Hankel matrix, we first assume the original signal is a noise-free, discrete sinusoidal signal sampled at a constant period t, which is given by $y(n) = a\sin(wtn+\varphi_0)$, where a, w, and φ_0 are the amplitude, frequency, and initial phase offset of the sinusoidal signal, respectively.

For convenience, we define

$$\vec{S}_p^q \doteq [\sin(wtp+\varphi_0), \sin(wt(p+1)+\varphi_0), \ldots, \sin(wtq+\varphi_0)],$$

and rewrite the generalized Hankel matrix as

$$\boldsymbol{H} = a \cdot \left[\vec{S}_1^{(n-r+1)}, \vec{S}_2^{(n-r+2)}, \cdots, \vec{S}_r^{n}\right]^T. \quad (10)$$

We also define

$$\vec{C}_p^q \doteq [\cos(wtp+\varphi_0), \cos(wt(p+1)+\varphi_0), \ldots, \cos(wtq+\varphi_0)].$$

Since $\sin(wt(n+1)+\varphi_0) = \sin(wtn+\varphi_0)\cos(wt) + \cos(wtn+\varphi_0)\sin(wt)$, we can convert the time-shift of Hankelization to a summation format. The generalized Hankel matrix $\boldsymbol{H}$ can be rewritten as

$$\boldsymbol{H} = a \cdot \begin{bmatrix} \vec{S}_1^{(n-r+1)}\cos(0) + \vec{C}_1^{(n-r+1)}\sin(0) \\ \vec{S}_1^{(n-r+1)}\cos(wt) + \vec{C}_1^{(n-r+1)}\sin(wt) \\ \vec{S}_1^{(n-r+1)}\cos(w2t) + \vec{C}_1^{(n-r+1)}\sin(w2t) \\ \cdots \\ \vec{S}_1^{(n-r+1)}\cos(w(r-1)t) + \vec{C}_1^{(n-r+1)}\sin(w(r-1)t) \end{bmatrix}.$$

Note that both vectors $[\cos(0), \cos(wt), \ldots, \cos(w(r-1)t)]$ and $[\sin(0), \sin(wt), \ldots, \sin(w(r-1)t)]$ are discrete sinusoidal signals with the same period w. Thus, we can rewrite $\boldsymbol{H}$ as $\boldsymbol{H} = \boldsymbol{\psi}_1^T \cdot \boldsymbol{\psi}_2$, where $\boldsymbol{\psi}_1 = [\alpha_1, \alpha_2]^T$ given by

$$\boldsymbol{\psi}_1 = 1 \cdot \begin{bmatrix} \cos(0), \cos(wt), \ldots, \cos(w(r-1)t) \\ \sin(0), \sin(wt), \ldots, \sin(w(r-1)t) \end{bmatrix}, \quad (11)$$

and $\boldsymbol{\psi}_2 = [\beta_1, \beta_2]^T$ given by

$$\boldsymbol{\psi}_2 = a \cdot \left[S_1^{(n-r+1)},\ C_1^{(n-r+1)} \right]^T, \quad (12)$$

where each row of $\boldsymbol{\psi}_1$ and $\boldsymbol{\psi}_2$ is a sinusoidal signal with period w. Therefore, both α_i and β_i are sinusoidal signals with the same period w. □

B. Discussion of Theorem 2

Since only the driver's breathing signal is captured by the phase difference sequence, the modified Hankel matrices can be regarded to be generated by a single sinusoidal signal (i.e., the breathing signal) plus noises from the driving environment. Following Theorem 1, the two related components should be decomposed, and thus we have $M \geqslant 2$.

Next we consider the upper bound of M to satisfy the uniqueness requirement of CPD. It is given that the output of CPD is unique only when $R_A + R_B + R_C \geq 2M + 2$ [47], where R_A, R_B, and R_C are the number of independent rows in matrix A, B, and C. In the constructed tensor, R_C is determined by the number of independent signals, while R_A and R_B are determined by the sampled signal used for hankelization. In our system, each tag can be considered as an independent sensor. So R_C equals to the number of deployed tags, which means $R_C \geqslant 4$ (since 4 to 8 tags are used). In addition, we have $R_A = R_B \geqslant 3$ because the breathing signal itself takes 2 rows and the noise in sampled data occupies at least one independent row. Therefore, to satisfy the uniqueness condition of CPD, we should have $2M+2 \leqslant \min\{R_A\}+\min\{R_B\}+\min\{R_C\} = 3+3+4 = 10$, i.e., $M \leqslant 4$. Thus, we conclude that the tensor rank used for CPD in the proposed system should satisfy $2 \leqslant M \leqslant 4$ and the CPD is unique.

REFERENCES

[1] National Highway Traffic Safety Administration. (2018). *U.S. DOT Announces 2017 Roadway Fatalities Down*. Accessed: Apr. 24, 2018. [Online]. Available: https://www.nhtsa.gov/press-releases/us-dot-announces-2017-roadway-fatalities-down

[2] Driver Knowledge. (2019). *Driving Facts*. Accessed: Apr. 25, 2016. [Online]. Available: https://www.driverknowledge.com/car-accident-statistics/

[3] B. Warwick, N. Symons, X. Chen, and K. Xiong, "Detecting driver drowsiness using wireless wearables," in *Proc. IEEE 12th Int. Conf. Mobile Ad Hoc Sensor Syst.*, Dallas, TX, USA, Oct. 2015, pp. 585–588.

[4] J. Solaz *et al.*, "Drowsiness detection based on the analysis of breathing rate obtained from real-time image recognition," *Transp. Res. Procedia*, vol. 14, pp. 3867–3876, Apr. 2016.

[5] H. Peng and W. Jia, "WiFind: Driver fatigue detection with fine-grained Wi-Fi signal features," in *Proc. IEEE Global Commun. Conf. (GLOBECOM)*, Singapore, Dec. 2017, pp. 1–6.

[6] Z. Yang, M. Bocca, V. Jain, and P. Mohapatra, "Contactless breathing rate monitoring in vehicle using UWB radar," in *Proc. 7th Int. Workshop Real-World Embedded Wireless Syst. Netw. (RealWSN)*, Shenzhen, China, Nov. 2018, pp. 13–18.

[7] X. Xu, J. Yu, Y. Chen, Y. Zhu, L. Kong, and M. Li, "Breathlistener: Fine-grained breathing monitoring in driving environments utilizing acoustic signals," in *Proc. 17th Annu. Int. Conf. Mobile Syst., Appl., Services*, Seoul, Republic of Korea, Jun. 2019, pp. 54–66.

[8] X. Wang, R. Huang, and S. Mao, "SonarBeat: Sonar phase for breathing beat monitoring with smartphones," in *Proc. 26th Int. Conf. Comput. Commun. Netw. (ICCCN)*, Vancouver, BC, Canada, Jul. 2017, pp. 1–8.

[9] Y. Hou, Y. Wang, and Y. Zheng, "TagBreathe: Monitor breathing with commodity RFID systems," in *Proc. IEEE 37th Int. Conf. Distrib. Comput. Syst. (ICDCS)*, Atlanta, GA, USA, Jun. 2017, pp. 404–413.

[10] C. Yang, X. Wang, and S. Mao, "AutoTag: Recurrent variational autoencoder for unsupervised apnea detection with RFID tags," in *Proc. IEEE Global Commun. Conf. (GLOBECOM)*, Abu Dhabi, UAE, Dec. 2018, pp. 1–7.

[11] C. Yang, X. Wang, and S. Mao, "Unsupervised detection of apnea using commodity RFID tags with a recurrent variational autoencoder," *IEEE Access*, vol. 7, pp. 67526–67538, 2019.

[12] Z. Lin, M. Chen, and Y. Ma, "The augmented Lagrange multiplier method for exact recovery of corrupted low-rank matrices," 2010, *arXiv:1009.5055*. [Online]. Available: http://arxiv.org/abs/1009.5055

[13] F. Adib, H. Mao, Z. Kabelac, D. Katabi, and R. C. Miller, "Smart homes that monitor breathing and heart rate," in *Proc. 33rd Annu. ACM Conf. Hum. Factors Comput. Syst. (CHI)*, Seoul, Republic of Korea, 2015, pp. 837–846.

[14] P. Nguyen, X. Zhang, A. Halbower, and T. Vu, "Continuous and fine-grained breathing volume monitoring from afar using wireless signals," in *Proc. 35th Annu. IEEE Int. Conf. Comput. Commun.*, San Francisco, CA, USA, Apr. 2016, pp. 1–9.

[15] H. Abdelnasser, K. A. Harras, and M. Youssef, "UbiBreathe: A ubiquitous non-invasive WiFi-based breathing estimator," in *Proc. IEEE MobiHoc*, Hangzhou, China, Jun. 2015, pp. 277–286.

[16] Z. Yang, P. H. Pathak, Y. Zeng, X. Liran, and P. Mohapatra, "Vital sign and sleep monitoring using millimeter wave," *ACM Trans. Sensor Netw.*, vol. 13, no. 2, pp. 1–32, Jun. 2017.

[17] J. Liu, Y. Wang, Y. Chen, J. Yang, X. Chen, and J. Cheng, "Tracking vital signs during sleep leveraging Off-the-shelf WiFi," in *Proc. 16th ACM Int. Symp. Mobile Ad Hoc Netw. Comput. (MobiHoc)*, Hangzhou, China, 2015, pp. 267–276.

[18] S. Shi, Y. Xie, M. Li, A. X. Liu, and J. Zhao, "Synthesizing wider WiFi bandwidth for respiration rate monitoring in dynamic environments," in *Proc. IEEE INFOCOM*, Paris, France, Apr./May 2019, pp. 181–189.

[19] X. Wang, C. Yang, and S. Mao, "TensorBeat: Tensor decomposition for monitoring multiperson breathing beats with commodity WiFi," *ACM Trans. Intell. Syst. Technol.*, vol. 9, no. 1, p. 8, Sep. 2017.

[20] C. Chen *et al.*, "TR-BREATH: Time-reversal breathing rate estimation and detection," *IEEE Trans. Biomed. Eng.*, vol. 65, no. 3, pp. 489–501, Mar. 2018.

[21] H. Wang *et al.*, "Human respiration detection with commodity WiFi devices: Do user location and body orientation matter?" in *Proc. ACM Int. Joint Conf. Pervasive Ubiquitous Comput.*, Heidelberg, Germany, Sep. 2016, pp. 25–36.

[22] X. Wang, C. Yang, and S. Mao, "ResBeat: Resilient breathing beats monitoring with realtime bimodal CSI data," in *Proc. IEEE GLOBECOM*, Singapore, Dec. 2017, pp. 1–6.

[23] Y. Zeng, D. Wu, R. Gao, T. Gu, and D. Zhang, "Fullbreathe: Full human respiration detection exploiting complementarity of CSI phase and amplitude of WiFi signals," *Proc. ACM Interact., Mobile, Wearable Ubiquitous Technol.*, vol. 2, no. 3, p. 148, Sep. 2018.
[24] R. Zhao, D. Wang, Q. Zhang, H. Chen, and A. Huang, "CRH: A contactless respiration and heartbeat monitoring system with COTS RFID tags," in *Proc. 15th Annu. IEEE Int. Conf. Sens., Commun., Netw. (SECON)*, Hong Kong, Jun. 2018, pp. 1–9.
[25] J. Liu, X. Chen, S. Chen, X. Liu, Y. Wang, and L. Chen, "TagSheet: Sleeping posture recognition with an unobtrusive passive tag matrix," in *Proc. IEEE INFOCOM*, Paris, France, Apr./May 2019, pp. 874–882.
[26] C. Wang, L. Xie, W. Wang, Y. Chen, Y. Bu, and S. Lu, "RF-ECG: Heart rate variability assessment based on COTS RFID tag array," *Proc. ACM Interact., Mobile, Wearable Ubiquitous Technol.*, vol. 2, no. 2, p. 85, Jun. 2018.
[27] L. Yang, Y. Chen, X.-Y. Li, C. Xiao, M. Li, and Y. Liu, "Tagoram: Real-time tracking of mobile RFID tags to high precision using COTS devices," in *Proc. 20th Annu. Int. Conf. Mobile Comput. Netw.*, Maui, HI, USA, Sep. 2014, pp. 237–248.
[28] C. Yang, X. Wang, and S. Mao, "SparseTag: high-precision backscatter indoor localization with sparse RFID tag arrays," in *Proc. 16th Annu. IEEE Int. Conf. Sens., Commun., Netw. (SECON)*, Boston, MA, USA, Jun. 2019, pp. 1–9.
[29] C. Zhao *et al.*, "RF-mehndi: A fingertip profiled RF identifier," in *Proc. IEEE Conf. Comput. Commun. (INFOCOM)*, Paris, France, Apr. 2019, pp. 1513–1521.
[30] J. Wang, J. Xiong, X. Chen, H. Jiang, R. K. Balan, and D. Fang, "TagScan: Simultaneous target imaging and material identification with commodity RFID devices," in *Proc. 23rd Annu. Int. Conf. Mobile Comput. Netw.*, Snowbird, UT, USA, Oct. 2017, pp. 288–300.
[31] T. Wei and X. Zhang, "Gyro in the air: Tracking 3D orientation of batteryless Internet-of-Things," in *Proc. 22nd Annu. Int. Conf. Mobile Comput. Netw.*, New York, NY, USA, Oct. 2016, pp. 55–68.
[32] P. Li, Z. An, L. Yang, and P. Yang, "Towards physical-layer vibration sensing with RFIDs," in *Proc. IEEE Conf. Comput. Commun. (INFOCOM)*, Paris, France, Apr. 2019, pp. 892–900.
[33] J. Guo, T. Wang, Y. He, M. Jin, C. Jiang, and Y. Liu, "Twinleak: RFID-based liquid leakage detection in industrial environments," in *Proc. IEEE Conf. Comput. Commun.*, Paris, France, Apr. 2019, pp. 883–891.
[34] J. Zhang, Z. Yu, X. Wang, Y. Lyu, S. Mao, S. C. Periaswamy, J. Patton, and X. Wang, "RFHUI: An intuitive and easy-to-operate human-uav interaction system for controlling a UAV in a 3D space," in *Proc. 15th EAI Int. Conf. Mobile Ubiquitous Syst., Comput., Netw. Services*, New York, NY, USA, Nov. 2018, pp. 69–76.
[35] J. Zhang *et al.*, "Robust RFID based 6-DoF localization for unmanned aerial vehicles," *IEEE Access*, vol. 7, pp. 77348–77361, 2019.
[36] L. M. Ni, Y. Liu, Y. Cho Lau, and A. P. Patil, "LANDMARC: Indoor location sensing using active RFID," in *Proc. 1st IEEE Int. Conf. Pervas. Comput. Commun. (PerCom)*, Dallas, TX, USA, Mar. 2003, pp. 407–415.
[37] W. Jue and D. Katabi, "Dude, where's my card? RFID positioning that works with multipath and non-line of sight," *ACM SIGCOMM Comput. Commun. Rev.*, vol. 43, no. 4, pp. 51–62, Aug. 2013.
[38] L. Shangguan and K. Jamieson, "The design and implementation of a mobile RFID tag sorting robot," in *Proc. 14th Annu. Int. Conf. Mobile Syst., Appl., Services (MobiSys)*, Singapore, 2016, pp. 31–42.
[39] Y. Ma, N. Selby, and F. Adib, "Minding the billions: Ultra-wideband localization for deployed RFID tags," in *Proc. 23rd Annu. Int. Conf. Mobile Comput. Netw.*, Snowbird, UT, USA, Oct. 2017, pp. 248–260.
[40] *Low Level User Data Support*, Impinj, Seattle, WA, USA, USA, Note, Impinj Speedway Revolution Reader Application, 2013.
[41] X. Wang, C. Yang, and S. Mao, "PhaseBeat: Exploiting CSI phase data for vital sign monitoring with commodity WiFi devices," in *Proc. IEEE 37th Int. Conf. Distrib. Comput. Syst. (ICDCS)*, Atlanta, GA, USA, Jun. 2017, pp. 1230–1239.
[42] C. Duan, L. Yang, H. Jia, Q. Lin, Y. Liu, and L. Xie, "Robust spinning sensing with Dual-RFID-Tags in noisy settings," in *Proc. IEEE Conf. Comput. Commun. (INFOCOM)*, Honolulu, HI, USA, Apr. 2018, PP. 855–863.
[43] L. Yang, Y. Li, Q. Lin, X.-Y. Li, and Y. Liu, "Making sense of mechanical vibration period with sub-millisecond accuracy using backscatter signals," in *Proc. 22nd Annu. Int. Conf. Mobile Comput. Netw.*, New York, NY, USA, Oct. 2016, pp. 16–28.
[44] X. Wang, J. Zhang, Z. Yu, S. Mao, S. C. G. Periaswamy, and J. Patton, "On remote temperature sensing using commercial UHF RFID tags," *IEEE Internet Things J.*, vol. 6, no. 6, pp. 10715–10727, Dec. 2019.
[45] J. Liu, P. Musialski, P. Wonka, and J. Ye, "Tensor completion for estimating missing values in visual data," *IEEE Trans. Pattern Anal. Mach. Intell.*, vol. 35, no. 1, pp. 208–220, Jan. 2013.
[46] A. Cichocki *et al.*, "Tensor decompositions for signal processing applications: From two-way to multiway component analysis," *IEEE Signal Process. Mag.*, vol. 32, no. 2, pp. 145–163, Mar. 2015.
[47] T. G. Kolda and B. W. Bader, "Tensor decompositions and applications," *SIAM Rev.*, vol. 51, no. 3, pp. 455–500, Aug. 2009.

Chao Yang (Student Member, IEEE) received the B.S. degree in electrical engineering from Yanshan University, Hebei, China, in 2015, and the M.S. degree in electrical and computer engineering (ECE) from Auburn University, Auburn, AL, in 2017, where he is currently pursuing the Ph.D. degree in ECE. His current research interests include health sensing, indoor localization, the Internet of Things, and wireless networks. He was a co-recipient of the Best Paper Award of IEEE GLOBECOM 2019.

Xuyu Wang (Member, IEEE) received the B.S. degree in electronic information engineering and the M.S. degree in signal and information processing from Xidian University, Xi'an, China, in 2009 and 2012, respectively, and the Ph.D. degree in electrical and computer engineering from Auburn University, Auburn, AL, USA, in August 2018. He is currently an Assistant Professor with the Department of Computer Science, California State University, Sacramento, CA. His research interests include indoor localization, deep learning, and big data. He was a co-recipient of the Second Prize of Natural Scientific Award of Ministry of Education, China, in 2013, the Best Paper Award of IEEE GLOBECOM 2019, The 2018 Best Journal Paper Award of IEEE Communications Society Multimedia Communications Technical Committee, the Best Demo Award of IEEE SECON 2017, and the Best Student Paper Award of IEEE PIMRC 2017.

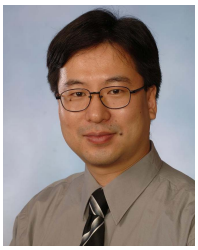

Shiwen Mao (Fellow, IEEE) received the Ph.D. degree in electrical and computer engineering from Polytechnic University, Brooklyn, NY, in 2004. He is currently the Samuel Ginn Endowed Professor with the Department of Electrical and Computer Engineering, and the Director of the Wireless Engineering Research and Education Center, Auburn University, Auburn, AL, USA. His research interests include wireless networks, multimedia communications, and smart grid.

Dr. Mao received the IEEE ComSoc TC-CSR Distinguished Technical Achievement Award in 2019, the IEEE ComSoc MMTC Distinguished Service Award in 2019, Auburn University Creative Research and Scholarship Award in 2018, the 2017 IEEE ComSoc ITC Outstanding Service Award, the 2015 IEEE ComSoc TC-CSR Distinguished Service Award, the 2013 IEEE ComSoc MMTC Outstanding Leadership Award, and NSF CAREER Award in 2010. He was also a co-recipient of the IEEE Vehicular Technology Society 2020 Jack Neubauer Memorial Award, the 2018 IEEE ComSoc MMTC Best Journal Paper Award, the 2017 IEEE ComSoc MMTC Best Conference Paper Award, the Best Demo Award from IEEE SECON 2017, the Best Paper Awards from IEEE GLOBECOM 2019, 2016, and 2015, IEEE WCNC 2015, and IEEE ICC 2013, and the 2004 IEEE Communications Society Leonard G. Abraham Prize in the Field of Communications Systems. He is an Area Editor of the IEEE TRANSACTIONS ON WIRELESS COMMUNICATIONS, IEEE OPEN JOURNAL OF THE COMMUNICATIONS SOCIETY, IEEE INTERNET OF THINGS JOURNAL, IEEE/CIC CHINA COMMUNICATIONS, and *ACM GetMobile*, and an Associate Editor of the IEEE TRANSACTIONS ON NETWORK SCIENCE AND ENGINEERING, IEEE TRANSACTIONS ON MOBILE COMPUTING, IEEE MULTIMEDIA, AND IEEE NETWORKING LETTERS, among others.